

Provided for non-commercial research and education use.
Not for reproduction, distribution or commercial use.



(This is a sample cover image for this issue. The actual cover is not yet available at this time.)

This article appeared in a journal published by Elsevier. The attached copy is furnished to the author for internal non-commercial research and education use, including for instruction at the authors institution and sharing with colleagues.

Other uses, including reproduction and distribution, or selling or licensing copies, or posting to personal, institutional or third party websites are prohibited.

In most cases authors are permitted to post their version of the article (e.g. in Word or Tex form) to their personal website or institutional repository. Authors requiring further information regarding Elsevier's archiving and manuscript policies are encouraged to visit:

<http://www.elsevier.com/copyright>



Contents lists available at SciVerse ScienceDirect

Computational Materials Science

journal homepage: www.elsevier.com/locate/commatsci

Surface stress effects on the critical buckling strains of silicon nanowires

Harold S. Park*

Department of Mechanical Engineering, Boston University, Boston, MA 02215, United States

ARTICLE INFO

Article history:

Received 15 June 2011

Received in revised form 18 July 2011

Accepted 27 July 2011

Keywords:

Surface stress

Buckling

Silicon nanowire

Surface Cauchy–Born

ABSTRACT

The objective of this paper is to quantify how nanoscale surface stresses impact the critical buckling strains of silicon nanowires. These insights are gained by using nonlinear finite element calculations based upon a multiscale, finite deformation constitutive model that incorporates nanoscale surface stress and surface elastic effects to study the buckling behavior of silicon nanowires that have cross sectional dimensions between 10 and 25 nm under axial compressive loading. The key finding is that, in contrast to existing surface elasticity solutions, the critical buckling strains are found to show little deviation from the classical bulk Euler solution. The present results suggest that accounting for axial strain relaxation due to surface stresses may be necessary to improve the accuracy and predictive capability of analytic linear surface elastic theories.

© 2011 Elsevier B.V. All rights reserved.

1. Introduction

Over the past decade, one-dimensional nanostructures such as nanowires have been extensively studied through both theory and experiment. The major impetus for this widespread interest is due to the novel optical, electrical, thermal and mechanical properties that these volume confined nanowires exhibit [1–3]. Due to these novel physical properties, nanowires are likely to be one of the major building blocks for future nanotechnologies and nanoelectromechanical systems (NEMS) [4–6]. For example, one emerging application of these silicon nanowires is for highly flexible and stretchable electronics [7,8]. While initial studies utilized micron-sized silicon structures [7], recent experimental work by Zhu et al. [9] utilized silicon nanowires with diameter averaging around 30 nm. As the trend for the size of electronics towards smaller size components, this suggests that the device performance of these stretchable electronics will be strongly dependent on how surface effects impact the buckling behavior and properties of the component silicon nanowires.

Because they will be a basic building block for NEMS, it will be critical to understand the mechanical properties of nanowires. As a result, there has been significant experimental and theoretical effort put forth to understand how and why the elastic properties of both metallic and semiconducting nanowires deviate from their bulk values [3]. While there is often disagreement between experiments, and also between experiments and theoretical predictions, there appears to be general agreement that the elastic properties of nanowires should be different from the bulk value due to the effect

of surface stresses [10], which act upon surface atoms due to their undercoordinated nature as compared to bulk atoms. Because surface atoms are undercoordinated, their elastic properties are expected to be different from bulk atoms [11], and thus as nanowires become smaller with a corresponding increase in surface area to volume ratio, the surface elastic properties are expected to have a significant impact on the overall elastic properties of the nanowires.

There exist several different approaches to experimentally measure the elastic properties of nanomaterials, including tension, resonance and bending. All of these approaches have been utilized in recent experiments to measure the elastic properties of nanowires [3]. Another fundamental measurement to obtain elastic properties is buckling, which is generally obtained through uniaxial compression of the nanowire. Recently, experimental studies of the buckling of silver [12], silicon [13–15,9] and ZnO nanowires [16–18] have all been reported. Similarly, several theoretical studies, which have generally been performed using classical molecular dynamics (MD) simulations have also been reported for the buckling of various nanowires, including FCC metals [19–21], iron [22], gallium nitride [23] and silicon [24]. We also note the recent analytic work of Wang and Feng [25] and Song et al. [26], who developed different models to estimate the change in critical buckling force if surface stress and surface elastic effects are considered.

With regards to the buckling investigations, most experimental studies [17,13,15] have focused on larger cross section nanowires (50–200 nm), where surface effects may be minimal. In contrast, the atomistic studies have been limited to very small (less than 10 nm) nanowire cross sections [24,23,19,22,20,21]. Therefore, there is currently lacking a systematic understanding of how nanoscale surface effects impact the critical buckling strains of

* Tel.: +1 617 353 4208; fax: +1 617 353 5866.

E-mail address: parkhs@bu.edu

nanowires, particularly when different geometries and cross sectional sizes that range between those studied experimentally and atomistically are considered. It is worth emphasizing that the relative lack of understanding as to how surface effects impact the buckling of nanowires is in stark contrast to the extensive literature that has recently developed regarding the buckling behavior of other nanostructures, especially carbon nanotubes [27–33].

This work aims to address the following issues, namely what effect do surface stresses, nanowire size and aspect ratio have on the critical buckling strains of silicon nanowires. These results are obtained using the recently developed surface Cauchy–Born (SCB) model, which is a multiscale, nonlinear constitutive model that incorporates surface stresses on nanostructures within a nonlinear finite element (FE) framework [34]. We compare all results for a given nanowire geometry both to buckling strains obtained from linear Euler buckling theory, which does not account for surface effects, and to recent analytic buckling models that do explicitly account for surface effects [25] to understand how surface effects impact the buckling strains as a function of nanowire size and geometry.

2. Surface Cauchy–Born model

2.1. Overview

The standard bulk Cauchy–Born (BCB) model is a multiscale, finite deformation constitutive model that enables the calculation of continuum stress and stiffness directly from an underlying interatomic potential energy [35,29,36,34,37,38]. However, because the BCB model does not account for critical nanoscale surface stress effects, the SCB model was recently developed for silicon nanostructures by Park and Klein [34] to capture surface stress effects within the framework of the Cauchy–Born approximation. Because the SCB formulation for silicon was presented in previous works by Park et al. [34,39,40], we refer the interested reader to those works for a detailed exposition on the SCB model.

In general, the SCB model augments the bulk strain energy density that is present in the BCB model with a surface strain energy density that represents the energy for a representative surface unit cell. The key to the SCB model is obtaining a total potential energy through the sum of the bulk and surface energy densities. By doing so, the total potential energy can be minimized using standard nonlinear FE techniques, which enables the application of the SCB model to three-dimensional boundary value problems involving nanomaterials while still accounting for the effects of nanoscale surface stresses and their effects on surface elastic properties. We also note that because the SCB and BCB are both nonlinear constitutive models, the effects of any deformation that results in the nanowire bulk due to surface stresses is naturally imparted to the bulk stress and stiffness; previous studies have indicated that such nonlinear deformation of the bulk may have a critical effect in the resulting nanowire elastic properties [41,42]. Finally, we note that thermal effects were not considered in the present work, though previous research has incorporated thermal effects on both the bulk and surface stresses into the SCB model [43].

3. Numerical examples

All numerical examples were performed on three-dimensional, single crystal silicon nanowires of length L and square cross section of width a . Three different parametric studies are conducted in this work, which consider nanowires with constant cross sectional area (CCSA), where $a = 10$ nm and $a = 25$ nm, and constant aspect ratio (CAR) of $L/a = 15$; the geometries are summarized in Table 1. All

Table 1

Summary of silicon nanowire geometries considered: constant aspect ratio (CAR), and constant cross sectional area (CCSA). All dimensions are in nanometers.

CAR	CCSA1	CCSA2
150 × 10 × 10	100 × 10 × 10	375 × 25 × 25
225 × 15 × 15	200 × 10 × 10	750 × 25 × 25
300 × 20 × 20	300 × 10 × 10	1125 × 25 × 25
375 × 25 × 25	400 × 10 × 10	

simulations were performed using the Sandia-developed simulation code Tahoe [44].

All nanowires had a (100) longitudinal orientation with unreconstructed {100} transverse surfaces, and were discretized using regular meshes of 8-node hexahedral elements, with at least 10 finite elements through the nanowire thickness. The underlying interatomic potential that was utilized for the SCB calculations for silicon is the T3 model of Tersoff [45].

The compressive loading was applied by prescribing a fixed displacement increment at both the $+x$ and $-x$ ends of the nanowire of ranging from 0.1 Å to 0.5 Å, at which point the interior of the nanowire was allowed to relax in response to the applied displacement to find an energy minimizing configuration. The loaded planes were not allowed to deform in either the y or z directions; as noted by Guo et al. [30], restricting in-plane (y and z) displacements are expected to lead to higher buckling strains as compared to the case where in-plane displacements are allowed.

After each displacement increment was applied and the nanowire had relaxed to the energy minimizing configuration, the stability of the nanowire was evaluated by finding the smallest eigenvalue of the FE stiffness matrix, where the buckling strain was determined from the point where the smallest eigenvalue of the FE stiffness matrix becomes negative, which is equivalent to the point at which the FE stiffness matrix loses positive definiteness [30]. We emphasize that through the usage of the nonlinear, finite deformation SCB model, changes in elasticity of both the bulk and surface due to deformation caused by the applied uniaxial loading as well as due to surface stresses are naturally captured by the FE stiffness matrix.

The boundary value problem thus corresponds to nanowires that are doubly-fixed; this would correspond to nanowires that are fabricated experimentally using a top-down etching approach, as is commonly done for silicon-based NEMS [5]. The effect of the doubly-fixed boundary conditions is that the axial length of the nanowires is fixed in the initial configuration; therefore, the silicon nanowires are effectively under compression as the nanowires are unable to expand axially to relieve the effects of the compressive silicon surface stresses [46,40]. As we will show, the critical buckling strains of the nanowires are strongly dependent on whether these axial strains due to surface stresses are accounted for or not.

We also compare our results to those that can be obtained from linear elastic Euler beam theory. As is well known, the buckling formula for a nanowire (beam) that is fixed at one end and axially compressed at the other end can be written as

$$P_{cr} = \frac{\pi^2 EI}{(Kl)^2}, \quad (1)$$

where P_{cr} is the critical force, E is the Young's modulus of the nanowire, I is the moment of inertia, l is the nanowire length, and K is a dimensionless coefficient known as the effective-length factor. For a nanowire (beam) that is fixed at both ends, as in the present numerical examples, $K = 0.5$.

To compare with the buckling strains obtained through the FE calculations in the present work, we rewrite Eq. (1) to solve for

Table 2
Summary of critical buckling strains (in percent) obtained using linear Euler buckling theory (ϵ_{cr}^{euler}) from Eq. (2) for CCSA nanowires as compared to surface Cauchy–Born calculations (ϵ_{cr}^{scb}) for silicon nanowires. The normalized effective Young's modulus E^{eff}/E for each geometry was calculated using both the analytic solution of He and Lilley (HL) [47], and the SCB model. The surface stress-induced axial strain ϵ_{scb}^{relax} was calculated using the SCB model using fixed/free boundary conditions for each geometry, while $\epsilon_{cr}^{scb(tot)} = \epsilon_{cr}^{scb} + \epsilon_{scb}^{relax}$.

Geometry	ϵ_{cr}^{euler}	ϵ_{cr}^{scb}	$\epsilon_{cr}^{scb} / \epsilon_{cr}^{euler}$	$\frac{E^{eff}}{E}$ (SCB)	$\frac{E^{eff}}{E}$ (HL)	ϵ_{scb}^{relax}	$\epsilon_{cr}^{scb(tot)} / \epsilon_{cr}^{euler}$
100 × 10 × 10	3.299	3.26	0.988	1.017	0.870	0.18	1.043
200 × 10 × 10	0.822	0.67	0.815	0.863	0.694	0.1915	1.048
300 × 10 × 10	0.366	0.187	0.511	0.546	0.399	0.1953	1.044
400 × 10 × 10	0.206	0.018	0.087	0.087	−0.019	0.1972	1.044

Table 3
Summary of critical buckling strains (in percent) obtained using linear Euler buckling theory (ϵ_{cr}^{euler}) from Eq. (2) for CCSA nanowires as compared to surface Cauchy–Born calculations (ϵ_{cr}^{scb}) for silicon nanowires. The normalized effective Young's modulus E^{eff}/E for each geometry was calculated using both the analytic solution of He and Lilley (HL) [47], and the SCB model. The surface stress-induced axial strain ϵ_{scb}^{relax} was calculated using the SCB model using fixed/free boundary conditions for each geometry, while $\epsilon_{cr}^{scb(tot)} = \epsilon_{cr}^{scb} + \epsilon_{scb}^{relax}$.

Geometry	ϵ_{cr}^{euler}	ϵ_{cr}^{scb}	$\epsilon_{cr}^{scb} / \epsilon_{cr}^{euler}$	$\frac{E^{eff}}{E}$ (SCB)	$\frac{E^{eff}}{E}$ (HL)	ϵ_{scb}^{relax}	$\epsilon_{cr}^{scb(tot)} / \epsilon_{cr}^{euler}$
375 × 25 × 25	1.462	1.413	0.967	0.987	0.919	0.0792	1.021
750 × 25 × 25	0.3655	0.299	0.818	0.823	0.761	0.0825	1.043
1125 × 25 × 25	0.1625	0.085	0.523	0.525	0.495	0.0836	1.038

the critical Euler buckling strain ϵ_{cr}^{euler} . This is done by noting that $P_{cr} = E \epsilon_{cr}^{euler} A$, and solving for the buckling strain to obtain

$$\epsilon_{cr}^{euler} = \frac{4\pi^2 I}{Al^2}, \quad (2)$$

where A is the cross sectional area of the nanowire. Importantly, we note that the buckling strain in Eq. (2) is independent of any material properties, i.e. the Young's modulus, and instead depends only on the geometry of the nanowire (beam).

4. Numerical results

We summarize in Tables 2–4 the critical buckling strains for both the BCB and SCB calculations for the CAR and CCSA geometries of the silicon nanowires as compared to the predictions obtained using the linear Euler buckling estimate given in Eq. (2). Table 2 demonstrates the expected result from Euler buckling theory, i.e. that the buckling strain decreases rapidly based on a $1/l^2$ relationship (see Eq. (2)) as the nanowire length l increases.

Tables 2–4 also show values for the normalized effective Young's modulus E_{eff}/E for each nanowire geometry, which was calculated using two different means. These normalized values were first obtained by calculating the resonant frequencies of the nanowires for each geometry by allowing them to relax, under fixed/ fixed boundary conditions, to a minimum energy configuration while accounting for surface stress effects and without any externally applied loading; this SCB-based procedure is identical to that utilized by Park [40] to calculate the elastic properties of silicon nanowires by relating the obtained resonant frequencies to the nanowire Young's modulus using well-known beam theory solutions for fixed/ fixed beams. The obtained E_{eff} from this procedure

was then normalized by the bulk Young's modulus of $\langle 100 \rangle$ silicon, which is 90.44 GPa using the parameters for the T3 version of the Tersoff potential [45].

The effective Young's modulus was also obtained for each geometry by using the recently obtained analytic solution of He and Lilley (HL) [47]. This particular model was chosen as it is obtained from the same set of governing Young–Laplace equations as was solved by Wang and Feng (WF) [25] to obtain estimates for the critical buckling force on nanostructures including surface effects, and because we will compare the presently obtained SCB results to the WF model in the next section. The HL effective Young's modulus shows similar trends as the SCB for each geometry, namely that the surface effects soften the material, and that an enhancement in surface-induced elastic softening is observed for both larger aspect ratios, and smaller nanowire cross sectional sizes. Also worth emphasizing is the fact that the effective Young's modulus obtained using the HL solution is always softer for the same geometry than the effective Young's modulus obtained using the SCB model; the relevance of this will be made clear in the following section. We note that similar trends have been recently found in experimental studies of the Young's modulus of silicon nanowires, where significant elastic softening with decreasing nanowire diameter have been reported for $\langle 110 \rangle$, $\langle 111 \rangle$ and $\langle 112 \rangle$ oriented silicon nanowires by various researchers [48,49,3,50,51].

We find in comparing the SCB results to the Euler results in Tables 2 and 3 that there are significant differences between the critical buckling strains predicted for the doubly-fixed CCSA silicon nanowires that are not allowed to expand axially in response to surface stress effects. Particularly noteworthy is the fact that, as the nanowire aspect ratio increases for both the CCSA1 geometries in Table 2 and the CCSA2 geometries in Table 3, the nanowire buck-

Table 4
Summary of critical buckling strains (in percent) obtained using linear Euler buckling theory (ϵ_{cr}^{euler}) from Eq. (2) for CAR nanowires as compared to surface Cauchy–Born calculations (ϵ_{cr}^{scb}) for silicon nanowires. The normalized effective Young's modulus E^{eff}/E for each geometry was calculated using both the analytic solution of He and Lilley (HL) [47], and the SCB model. The surface stress-induced axial strain ϵ_{scb}^{relax} was calculated using the SCB model using fixed/free boundary conditions for each geometry, while $\epsilon_{cr}^{scb(tot)} = \epsilon_{cr}^{scb} + \epsilon_{scb}^{relax}$.

Geometry	ϵ_{cr}^{euler}	ϵ_{cr}^{scb}	$\epsilon_{cr}^{scb} / \epsilon_{cr}^{euler}$	$\frac{E^{eff}}{E}$ (SCB)	$\frac{E^{eff}}{E}$ (HL)	ϵ_{scb}^{relax}	$\epsilon_{cr}^{scb(tot)} / \epsilon_{cr}^{euler}$
150 × 10 × 10	1.462	1.347	0.921	0.966	0.797	0.1876	1.049
225 × 15 × 15	1.462	1.387	0.949	0.973	0.865	0.1287	1.038
300 × 20 × 20	1.462	1.413	0.967	0.981	0.899	0.0981	1.033
375 × 25 × 25	1.462	1.413	0.967	0.987	0.919	0.0792	1.021

ling strain decreases dramatically as compared to the Euler value. Furthermore, it is interesting to note that the ratio of buckling strains $\epsilon_{cr}^{scb}/\epsilon_{cr}^{euler}$ in Tables 2 and 3 appear to be related to the corresponding decrease in elastic stiffness due to surface effects as shown by comparing to the E^{eff}/E ratios.

However, it is important to note that the critical buckling strains ϵ_{cr}^{scb} are not measured from a stress-free configuration; as previously discussed in a variety of works [52,53,40,54,55], the bulk lattice constant does not correspond to the stress-free configuration for nanowires due to the effects of surface stress. Specifically, the zero stress configuration for FCC metal nanowires is a reduced lattice constant because the nanowires must contract in response to the tensile metallic surface stresses [52–55]. In contrast, the zero stress configuration for silicon nanowires requires a larger lattice constant because the nanowires must expand in response to the compressive silicon surface stresses [34,40,56].

Therefore, we also calculate the critical buckling strains from the zero stress configuration, i.e. the one where axial elongation due to surface stresses ϵ_{scb}^{relax} in Tables 2–4 is accounted for. In other words, the reference configuration is one in which the lattice constant of the nanowire is larger due to the expansion of the fixed/free silicon nanowire caused by the surface stresses. If the critical buckling strain is measured from this configuration, then as shown in Tables 2–4 the buckling strains accounting for surface stress and surface elastic effects ($\epsilon_{cr}^{scb(tot)}/\epsilon_{cr}^{euler}$) show little difference from that expected from classical Euler beam theory, which does not account for surface effects.

Table 4 shows the results for the CAR geometries. The rationale for choosing this geometry is clearly illustrated in the Euler buckling results in Table 4, where despite the changes in nanowire cross sectional area, the critical buckling strain of $\epsilon = 1.462\%$ as predicted by linear Euler theory remains constant for all CAR nanowire geometries. In contrast, when surface effects are accounted for on the doubly fixed silicon nanowires, there is a nearly 10% difference in critical buckling strain ($\epsilon_{cr}^{scb}/\epsilon_{cr}^{euler}$) for the smallest cross section ($a = 10$ nm) nanowire in Table 4, where the reduction in buckling strain with decreasing nanowire cross section follows a similar trend as observed for the effective Young's modulus E^{eff}/E . However, we note that the effect of surfaces on the critical buckling strain is clearly observed in Table 4 to decrease, as expected, as ϵ_{cr}^{scb} approaches ϵ_{cr}^{euler} with increasing nanowire cross sectional dimension.

The strong effect of the surface stress-induced initial strain ϵ_{scb}^{relax} on the nanowire buckling strain is also shown in Table 4. In particular, when the relaxation strain that corresponds to a zero stress configuration is accounted for, the critical buckling strains accounting for surface effects ($\epsilon_{cr}^{scb(tot)}/\epsilon_{cr}^{euler}$) again show very little deviation from the classical bulk value, with the deviation becoming smaller with an increase in nanowire cross sectional dimensions.

5. Discussion

Recently, Wang and Feng [25] accounted for surface stress and surface elastic effects within the confines of the linear surface elastic theory of Gurtin and Murdoch [57] to analyze surface effects on the buckling behavior of nanostructures. Before moving forward, we recall that, in the surface elastic theory of Gurtin and Murdoch, the surface stress τ^0 and surface stiffness E^s can be written as

$$\tau(\epsilon) = \tau^0 + E^s \epsilon, \quad (3)$$

$$E^s = \left. \frac{\partial \tau}{\partial \epsilon} \right|_{\epsilon=0}, \quad (4)$$

where τ^0 is the residual (strain-independent) part of the surface stress τ and $E^s \epsilon$ is the surface elastic (strain-dependent) part of

the surface stress. Note that Eq. (3) is written in terms of the infinitesimal strain tensor ϵ .

Using this formalism, the WF model results in an equation to predict how the critical applied force P_{cr} would change if surface effects were considered. For the bulk material, the critical buckling load P_{cr}^{bulk} can be related to the critical buckling strain ϵ_{cr}^{bulk} through a procedure identical to that which was used to obtain Eq. (2), i.e.

$$P_{cr}^{bulk} = E \epsilon_{cr}^{bulk} A = \frac{4\pi^2 EI}{l^2}. \quad (5)$$

Similarly, the critical buckling force P_{cr}^{surf} accounting for surface effects is written as, modifying Eq. 11 in Wang and Feng [25]

$$P_{cr}^{surf} = E^{eff} \epsilon_{cr}^{surf} A = \frac{4\pi^2 (EI)^*}{l^2} + 2\tau^0 h, \quad (6)$$

where E^{eff} is the effective Young's modulus of the nanowire when surface effects are accounted for, ϵ_{cr}^{surf} is the critical buckling strain when surface effects are accounted for and $(EI)^*$ is given as

$$(EI)^* = \frac{Eh^4}{12} + \frac{E^s h^3}{2} + \frac{E^s h^3}{6}, \quad (7)$$

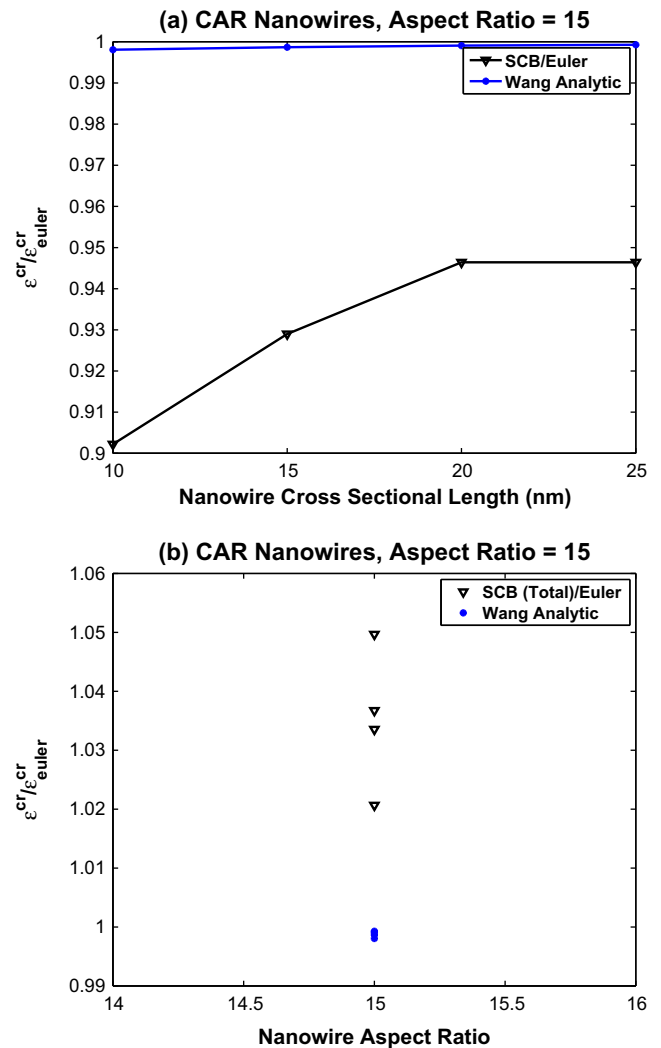


Fig. 1. Comparison of SCB to analytic WF solution for critical buckling strain of CAR silicon nanowires when tensile relaxation strains due to surface stresses: (a) are not accounted for in the SCB results; (b) are accounted for in the SCB results.

where h is the height of the nanowire cross section, and E^s is the surface elastic stiffness from Eq. (4). We note that values for E^{eff} for each nanowire geometry were previously given in Tables 2–4.

The ratio of critical buckling strains $\epsilon_{cr}^{surf} / \epsilon_{cr}^{bulk}$ can be obtained by dividing Eq. (6) by Eq. (5). In doing so, it is important to note that this ratio is dependent on the effective flexural rigidity (EI)^{*}. We will compare this analytic result to both the $\epsilon_{cr}^{scb} / \epsilon_{cr}^{euler}$ and $\epsilon_{cr}^{scb(tot)} / \epsilon_{cr}^{euler}$ ratios that were previously calculated for each nanowire geometry in Tables 2–4.

To evaluate the analytic equations in Eqs. (5) and (6), values for the surface stress and surface stiffness are needed. The surface stress and surface elastic constants for the Tersoff T3 potential, which we have utilized for the SCB simulations in this work, were recently evaluated by Izumi et al. [58]. They reported the following values: $\tau^0 = -0.88$ N/m and $E^s = -8.07$ N/m for unreconstructed {100} surfaces of silicon. We note that we have considered only the isotropic components of the surface stress and stiffness in the present work, which is an acceptable approximation for comparative purposes as the analytic expression of the WF model are based upon the one-dimensional (scalar) form of the surface stress and stiffness, and also because the buckling deformation is essentially one-dimensional (axial).

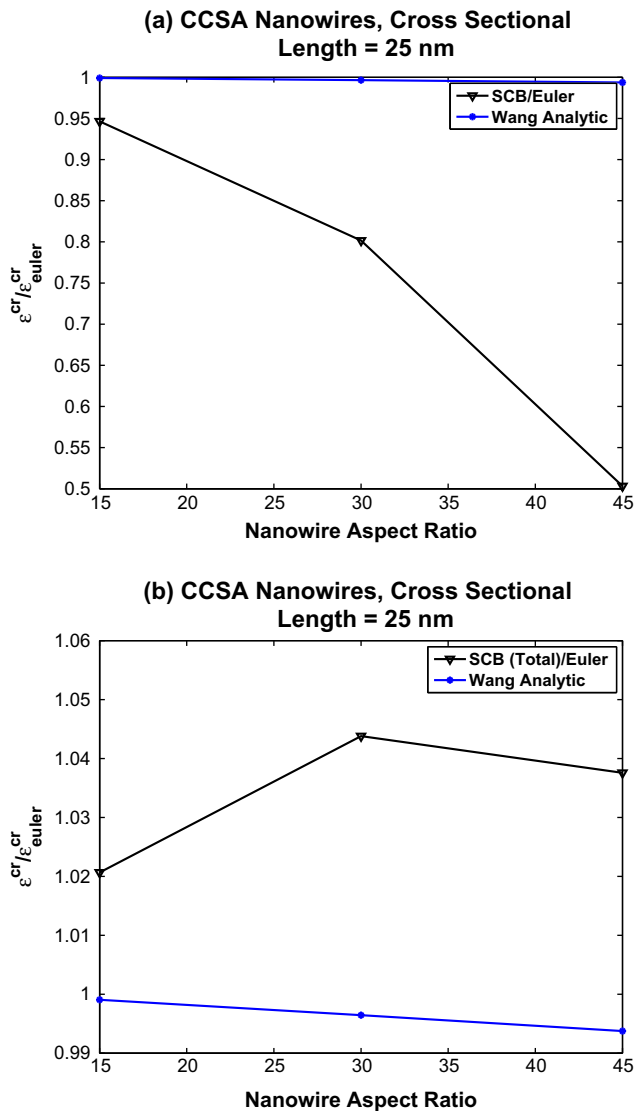


Fig. 2. Comparison of SCB to analytic WF solution for critical buckling strain of CCSA1 silicon nanowires when tensile relaxation strains due to surface stresses: (a) are not accounted for in the SCB results; (b) are accounted for in the SCB results.

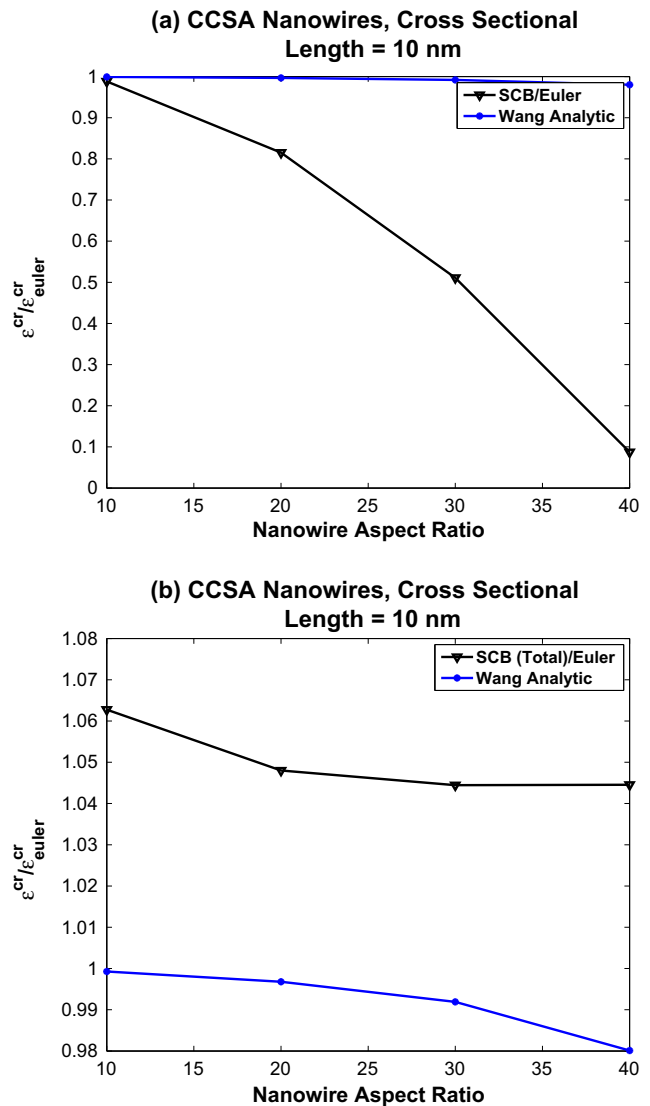


Fig. 3. Comparison of SCB to analytic WF solution for critical buckling strain of CCSA2 silicon nanowires when tensile relaxation strains due to surface stresses: (a) are not accounted for in the SCB results; (b) are accounted for in the SCB results.

We show comparisons in Figs. 1–3 between the two SCB results to the analytic WF model for all nanowire geometries considered. There are several interesting and salient points, which we now discuss.

First, it can be observed for all geometries that we have considered that the analytic solution of the WF model predicts that the critical buckling strains when surface effects are accounted for will be very slightly reduced as compared to that expected from classical Euler beam theory. Specifically, the largest deviation that is observed is about 2%, for the smaller (10 nm cross section) CCSA nanowires in Fig. 3b. We contrast the WF model results to the instability strains predicted using the SCB model for the fixed/fixed nanowires without accounting for the initial axial relaxation strains due to surface stresses ϵ_{scb}^{relax} ; these are found in Figs. 1a, 2a, and 3a. As can be seen in those figures, the SCB model predicts a significantly larger decrease in critical buckling strain for all nanowire geometries.

However, the situation appears on the surface to be different if the critical buckling strains for the SCB model are measured with respect to the zero stress reference configuration, where we have previously noted that capturing this axial tensile strain due to surface stresses has a significant effect on the critical buckling strain

that is predicted. Thus, we show in Figs. 1b, 2b and 3b that if the tensile relaxation strain due to surface stresses ϵ_{sch}^{relax} is accounted for in the SCB model, that the WF model and the SCB calculations give similar, though not identical, predictions for the bulk-normalized critical buckling strains, where the normalization for both the WF and SCB models was by the bulk critical Euler buckling strain. However, we should emphasize that this agreement is quite serendipitous because the analytic WF model, as previously noted, does not account for surface stress-induced axial strains. We also note the recent MD studies of the buckling of gold nanowires by Olsson and Park [21], who also found that the critical buckling strains showed very little deviation from the expected bulk Euler predictions, even for very small nanowire diameters (<5 nm). Overall, these comparisons suggest that existing linear surface elastic theories may need to account for axial strain relaxation due to surface stresses to improve their accuracy and predictive capabilities.

We also compare our results to existing experimental data on the buckling of silicon nanowires presented by Hsin et al. [13]. In that work, VLS-grown silicon nanowires with diameters ranging from 40 to 90 nm were compressed by pushing a tungsten probe against the nanowire. We note that the axial orientation of the nanowire was not specified, and that the nanowires considered had a 5 nm thick native oxide layer that is not accounted for in the current SCB calculations. In doing so, they found that the critical force needed to buckle the nanowires for the entire range of nanowire diameters agreed with that predicted from classical Euler theory. This finding correlates with what was found for the silicon nanowires in the present work, and implies that if axial strain due to surface stress are accounted for, as would be the case in VLS-grown nanowires, then the critical buckling strains are quite similar to those expected from classical Euler theory. However, we note that the diameters that were considered in the work of Hsin et al. are larger than what was considered in the present work. Therefore, it is possible that their nanowires were too large to exhibit surface effects, though we note that a plethora of recent experiments [3,51,50,40] have shown that silicon nanowires show a strong size-dependence in the elastic properties for nanowires with diameter below about 100 nm.

6. Conclusions

In conclusion, we have utilized recently developed nonlinear multiscale computational techniques to study the effects of surface stresses on the critical buckling strains of silicon nanowires with cross sectional sizes ranging from 10 to 25 nm. The key finding of the present work is that the buckling strains of nanowires are controlled by the initial state from which they are tested, where the initial state is strongly influenced by surface stress effects. Specifically, the critical buckling strains for doubly-fixed silicon nanowires, which cannot expand axially to relieve the effects of the compressive surface stresses of silicon, are significantly lower than that expected from classical Euler theory, which does not consider surface effects. In contrast, if the tensile axial strains due to surface stresses are accounted for, and buckling begins from a zero-stress configuration, then the critical buckling strains are found to show little deviation from that expected from Euler theory. Finally, comparisons to existing linear surface elastic theories suggest that accounting for axial strain relaxation due to surface stresses may be necessary to improve their accuracy and predictive capability.

Acknowledgment

H.S.P. acknowledges support from NSF Grant CMMI-0750395.

References

- [1] C.M. Lieber, Z.L. Wang, MRS Bulletin 32 (2007) 99–108.
- [2] Y. Xia, P. Yang, Y. Sun, Y. Wu, B. Mayers, B. Gates, Y. Yin, F. Kim, H. Yan, Advanced Materials 15 (2003) 353–389.
- [3] H.S. Park, W. Cai, H.D. Espinosa, H. Huang, MRS Bulletin 34 (2009) 178–183.
- [4] H.G. Craighead, Science 290 (2000) 1532–1535.
- [5] K.L. Ekinci, M.L. Roukes, Review of Scientific Instruments 76 (2005) 061101.
- [6] K. Eom, H.S. Park, D.S. Yoon, T. Kwon, Physics Reports 503 (2011) 115–163.
- [7] D.-Y. Khang, H. Jiang, Y. Huang, J.A. Rogers, Science 311 (2006) 208–212.
- [8] J.A. Rogers, T. Someya, Y. Huang, Science 327 (2010) 1603–1607.
- [9] F. Xu, W. Lu, Y. Zhu, ACS Nano 5 (2011) 672–678.
- [10] R.C. Cammarata, Progress in Surface Science 46 (1994) 1–38.
- [11] V.B. Shenoy, Physical Review B 71 (2005) 094104.
- [12] R. Gunawidjaja, H. Ko, C. Jiang, V.V. Tsukruk, Chemistry of Materials 19 (2007) 2007–2015.
- [13] C.-L. Hsin, W. Mai, Y. Gu, Y. Gao, C.-T. Huang, Y. Liu, L.-J. Chen, Z.-L. Wang, Advanced Materials 20 (2008) 3919–3923.
- [14] B. Li, M.K. Kang, K. Lu, R. Huang, P.S. Ho, R.A. Allen, M.W. Cresswell, Nano Letters 8 (2008) 92–98.
- [15] S.Y. Ryu, J. Xiao, W.I. Park, K.S. Son, Y.Y. Huang, U. Paik, J.A. Rogers, Nano Letters 9 (2009) 3214–3219.
- [16] L.-W. Ji, S.-J. Young, T.-H. Fang, C.-H. Liu, Applied Physics Letters 90 (2007) 033109.
- [17] M. Riaz, O. Nur, M. Willander, P. Klason, Applied Physics Letters 92 (2008) 103118.
- [18] M. Riaz, A. Faluti, L.L. Yang, O. Nur, M. Willander, P. Klason, Journal of Applied Physics 104 (2008) 104306.
- [19] H.A. Wu, A.K. Soh, International Journal of Nonlinear Sciences and Numerical Simulation 4 (2003) 233–238.
- [20] H.A. Wu, Computational Materials Science 31 (2004) 287–291.
- [21] P.A.T. Olsson, H.S. Park, Acta Materialia 59 (2011) 3883–3894.
- [22] P.A.T. Olsson, S. Melin, C. Persson, Physical Review B 76 (2007) 224112.
- [23] Z. Wang, X. Zu, L. Yang, F. Gao, W.J. Weber, Physica E 40 (2008) 561–566.
- [24] Y. Jing, Q. Meng, Y. Gao, Computational Materials Science 45 (2009) 321–326.
- [25] G.-F. Wang, X.-Q. Feng, Applied Physics Letters 94 (2009) 141913.
- [26] F. Song, G.L. Huang, H.S. Park, X.N. Liu, International Journal of Solids and Structures 48 (2011) 2154–2163.
- [27] A. Sears, R.C. Batra, Physical Review B 73 (2006) 085410.
- [28] A. Pantano, D.M. Parks, M.C. Boyce, Journal of the Mechanics and Physics of Solids 52 (2004) 789–821.
- [29] M. Arroyo, T. Belytschko, Journal of the Mechanics and Physics of Solids 50 (2002) 1941–1977.
- [30] X. Guo, A.Y.T. Leung, H. Jiang, X.Q. He, Y. Huang, Journal of Applied Mechanics 74 (2007) 347–351.
- [31] G. Cao, X. Chen, Nanotechnology 17 (2006) 3844–3855.
- [32] K.M. Liew, C.H. Wong, X.Q. He, M.J. Tan, S.A. Meguid, Physical Review B 69 (2004) 115429.
- [33] C. Li, T.-W. Chou, Mechanics of Materials 36 (2004) 1047–1055.
- [34] H.S. Park, P.A. Klein, Computer Methods in Applied Mechanics and Engineering 197 (2008) 3249–3260.
- [35] E. Tadmor, M. Ortiz, R. Phillips, Philosophical Magazine A 73 (1996) 1529–1563.
- [36] P. Zhang, Y. Huang, P.H. Geubelle, P.A. Klein, K.C. Hwang, International Journal of Solids and Structures 39 (2002) 3893–3906.
- [37] Z. Tang, H. Zhao, G. Li, N.R. Aluru, Physical Review B 74 (2006) 064110.
- [38] E.B. Tadmor, G.S. Smith, N. Bernstein, E. Kaxiras, Physical Review B 59 (1999) 235–245.
- [39] H.S. Park, Nanotechnology 20 (2009) 115701.
- [40] H.S. Park, Journal of Applied Physics 103 (2008) 123504.
- [41] H. Liang, M. Upmanyu, H. Huang, Physical Review B 71 (2005) 241403(R).
- [42] H.S. Park, P.A. Klein, Journal of the Mechanics and Physics of Solids 56 (2008) 3144–3166.
- [43] G. Yun, H.S. Park, Computer Methods in Applied Mechanics and Engineering 197 (2008) 3337–3350.
- [44] Tahoe, 2011. <<http://sourceforge.net/projects/tahoe/>>.
- [45] J. Tersoff, Physical Review B 39 (1989) 5566–5568.
- [46] H. Balamane, T. Halicioglu, W.A. Tiller, Physical Review B 46 (1992) 2250–2279.
- [47] J. He, C.M. Lilley, Nano Letters 8 (2008) 1798–1802.
- [48] X. Li, T. Ono, Y. Wang, M. Esashi, Applied Physics Letters 83 (2003) 3081–3083.
- [49] H. Sadeghian, C.K. Yang, J.F.L. Goosen, E. van der Drift, A. Bossche, P.J. French, F. van Keulen, Applied Physics Letters 94 (2009) 221903.
- [50] X. Han, K. Zheng, Y.F. Zhang, X. Zhang, Z. Zhang, Z.L. Wang, Advanced Materials 19 (2007) 2112–2118.
- [51] Y. Zhu, F. Xu, Q. Qin, W.Y. Fung, W. Lu, Nano Letters 9 (2009) 3934–3939.
- [52] H.S. Park, K. Gall, J.A. Zimmerman, Physical Review Letters 95 (2005) 255504.
- [53] J. Diao, K. Gall, M.L. Dunn, Nature Materials 2 (2003) 656–660.
- [54] W. Liang, M. Zhou, F. Ke, Nano Letters 5 (2005) 2039–2043.
- [55] H.S. Park, C. Ji, Acta Materialia 54 (2006) 2645–2654.
- [56] B. Lee, R.E. Rudd, Physical Review B 75 (2007) 195328.
- [57] M.E. Gurtin, A. Murdoch, Archives of Rational Mechanics and Analysis 57 (1975) 291–323.
- [58] S. Izumi, S. Hara, T. Kumagai, S. Sakai, Thin Solid Films 467 (2004) 253–360.